Eur. J. Mineral., 38, 655–667, 2026
https://doi.org/10.5194/ejm-38-655-2026
© Author(s) 2026. This work is distributed under
the Creative Commons Attribution 4.0 License.

European Journal of Mineralogy
Open Access

Asymmetrical compositional gap between muscovite and NH_4-bearing micas – structural constraints: a combined experimental–theoretical study

Fernando Nieto[1], Elizabeth Escamilla-Roa[2], Vicente Timón[3], Josefina Pedrajas[4], María del Mar Abad[4], and Blanca Bauluz[5]

[1]Departamento Mineralogia y Petrologia and IACT, Universidad de Granada, Avenida Fuente Nueva s/n, 18071 Granada, Spain
[2]Instituto Andaluz de Ciencias de la Tierra, CSIC, Av. de las Palmeras 4, 18100 Granada, Spain
[3]Instituto de Estructura de la Materia, CSIC, MADRID, C/ Serrano, 119, 28006 Madrid, Spain
[4]Centro de Instrumentación Científica, Universidad de Granada, Paseo Prof. Juan Ossorio s/n, 18071 Granada, Spain
[5]IUCA-Facultad de Ciencias, Universidad de Zaragoza, Pedro Cerbuna 12, Zaragoza, Spain

Correspondence: Fernando Nieto (nieto@ugr.es)

Received: 14 April 2026 – Revised: 9 September 2026 – Accepted: 24 September 2026 – Published: 5 November 2026

Abstract. The usual coexistence in nature and in synthesised samples of NH_4-bearing micas with NH_4-free muscovite or illite has brought us to study their structural stability and characteristics. We used a combination of density functional theory methods and updated absorption-corrected nanoscale analyses of previously studied Germunde (Portugal) and Iberian Range (Spain) samples. Energy dispersive X-ray compositional maps were acquired using high-resolution scanning transmission electron microscopy, with high-angle annular dark-field images of ion-milled samples. The maps show the micaceous areas formed by a nano-intergrowth of major ammonium mica and minor muscovite or illite. To avoid mutual contamination between the two types of micas, zones were selected on homogeneous areas of the maps. The computer simulation allowed the structure of tobelite and various NH_4/K ratio compositions to be reproduced and their energetic differences to be calculated. The overall range from pure tobelite up to $3K/1NH_4$ compositions is stable, but the composition $7K/1NH_4$ has positive cation exchange energy, being unstable. This composition coincides with a compositional gap found in the analysed real samples, which is responsible for the co-existence at the level of samples of NH_4-free micas with the ammonium micas. The computer calculation has confirmed the structural similarity between the two kinds of micas, with the exception of the interlayer space, where H bonds play a significant role in the stabilisation of the tobelite structure. As a difference compared to K micas, the NH_4 micas mix a variety of polytypes at the sample level. Ammonium micas cover a continuous solid solution from tobelite up to a composition with major K but still some NH_4; hence, they should be considered to be a series name, with minor structural differences compared to muscovite, separated by a compositional gap.

1 Introduction

Micas are abundant rock-forming minerals that are usually present in a variety of geological environments. Their structure includes silicate TOT (Tetrahedral–Octahedral–Tetrahedral) layers linked through ionic bonds by cations in the interlayer space. They are usually big monovalent or bivalent cations, which are called interlayer cations. The most frequent in nature is K, but Na and Ca are also frequent constituents, either in solid solution with K or as major components.

In sediments with high organic matter content or intercalation of coal beds, ammonium is also frequently an additional cation, which is finally incorporated in the interlayer space of micas formed by diagenetic/metamorphic processes. In them, may NH_4 partially or totally substitute K in the interlayer position. NH_4 mica can also be formed as a hydrothermal product (Bobos, 2012). Ammonium phyllosilicates have also been described in extraterrestrial environments (e.g. Ammannito et al., 2016). The NH_4 mica endmember was first described by Higashi (1982) and was named tobelite. In most of the samples, two micas (tobelite and muscovite) coexist at the nanometric scale (Nieto, 2002; Bauluz and Nieto, 2018).

As the proportion of NH_4 in the system can be very variable, depending not only on the sample but also on the particular location in a given sample, a complete solid-solution NH_4-K has been described and usually covers a wide range of K/NH_4 ratios at the level of the sample (Nieto, 2002; Bentabol and Ruiz Cruz, 2016b; Bauluz and Nieto, 2018; Bobos, 2019). When NH_4 micas are rock-forming minerals, they systematically coexist with normal illite and/or muscovite (Fig. 1). These co-existing K micas are apparently NH_4-free or must contain NH_4 in a very small proportion as their X-ray diffraction (XRD) characteristics, particularly the d_{001} spacing but also the intensity of the basal peak ratios, are systematically those of illite/muscovite, lacking the identifying characteristics of NH_4-bearing micas.

Interestingly, the two coexisting micas are (1) a solid-solution NH_4-K, with highly variable proportions between them, from nearly pure tobelite up to K as the major interlayer cation with minor NH_4, and (2) a nearly pure K mica (muscovite or illite endmember). This is anomalous in relation to other similar compositional gaps, for example, between muscovite and the Na mica (paragonite), where the two coexisting micas are paragonite (with some minor K) and muscovite (with some minor Na), absent in the compositions around 50 % : 50 % (Guidotti et al., 1994). This is the normal behaviour in most minerals showing solid solutions with a compositional gap, that is, with the two endmembers coexisting as separate minerals (see Fig. 3 in Nickel, 1992).

Based on the described X-ray diffraction (XRD) features and chemical compositions, Juster et al. (1987), Nieto (2002), and Bentabol and Ruiz Cruz (2016b) proposed the existence of the aforementioned compositional gap, but, to our knowledge, its chemical extension and structural characteristics have not been previously described.

Because tobelites (and NH_4-rich muscovites) have very small grain sizes and low crystallinity, their structural determination is challenging. To our knowledge, only Rietveld refinements (Harlov et al., 2001; Poter et al., 2007), two single-crystal determinations (Mesto et al., 2012), and refinement of cell parameters (Bentabol and Ruiz Cruz, 2016a) have been published. The configuration of the H atoms of NH_4 in the interlayer space is unknown because the quality of the structural determinations did not allow their refinement. In general, the structural parameters determined for tobelite or NH_4-rich muscovites are very similar to those of muscovites, with the only exception being the interlayer space, which changes linearly as a function of the interlayer cation size. This thickening of the interlayer space with bigger cations, such as NH_4, is clearly responsible for the increase in d_{00l}, which allows the differentiation between tobelite (or NH_4-bearing micas) and muscovite by XRD (Drits et al., 1997; Higashi, 2000). Another significant difference that helps the distinction between the two kinds of micas by XRD is their different intensity ratios of the (00l) peaks.

One interesting difference between the structural characteristics of K micas (muscovite and illite) and the NH_4-bearing ones relates to the polytypes. As is extensively known in the literature, mature dioctahedral micas (muscovite) tend to develop the most stable $2M_1$ polytype, which is attained through the progressive ordering of the disordered $1M_d$ polytype, which is usually described in illites (Chen and Wang, 2007; Nieto et al., 2010); the 1M polytype is restricted to particular compositions of the system (Peacor et al., 2002). Nevertheless, all of the selected-area electron diffractions (SAEDs) of NH_4-rich micas obtained by transmission electron microscopy (TEM) have found a mixture of two-layer, one-layer, and disordered polytypes at the sample level (Nieto, 2002; Bentabol and Ruiz Cruz, 2016b; Bauluz and Nieto, 2018; Bobos, 2019). The two crystals structurally determined by Mesto et al. (2012) corresponded to the $2M_2$ polytype, but, in a TEM study of the same sample, Capitani et al. (2016) concluded that it contained a partial mixture of polytypes. Rietveld analyses by Harlov et al. (2001) and Poter et al. (2007) showed that the synthesised micas comprised a complex mixture of 1M, $2M_1$, $2M_2$, 3T, and 2Or polytypes.

This study aims to explain the usual coexistence of two different micas (one NH_4-bearing and one NH_4-free), to determine the possible existence and location of a compositional gap between them, and to find their structural reasons. Natural samples were revisited, and first-principle calculations were performed to analyse the stability of different structural solutions. Several atomistic models were constructed by varying the interlayer cation (NH_4^+ and K^+) and considering their possible coexistence within the same structure. These models allow us to evaluate the influence of the nature and distribution of interlayer cations on the relative

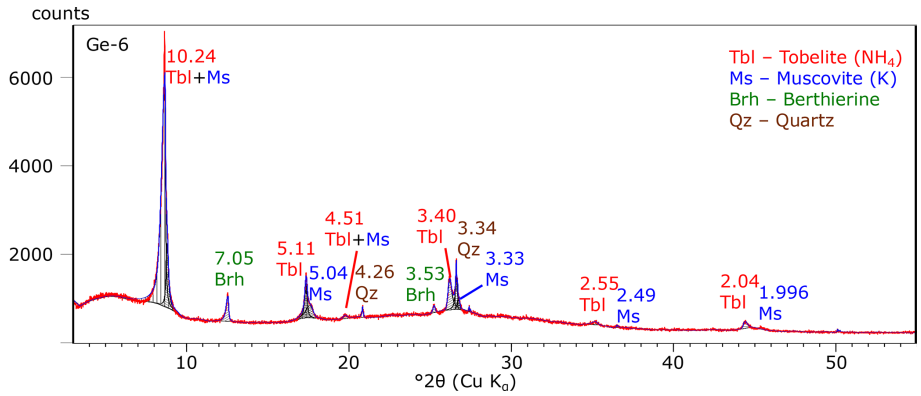


Figure 1. X-ray diffraction powder (oriented aggregate) diagram of the $< 2\,\mu m$ fraction of sample Ge-6, representative of natural samples containing NH_4-bearing micas. The two micas are recognisable by their slightly different basal spacings (NH_4-bearing mica indicated in red and K mica indicated in blue). Red line: experimental; hatched black areas: decomposed peaks; blue line: sum diagram of decomposed peaks.

stability, structural arrangement, and energetic favourability of the system. Furthermore, this approach provides insight into the likelihood of observing such mixed-cation configurations in natural samples, thereby bridging the gap between idealised models and the compositional complexity found in real tobelite clay minerals.

2 Samples and methods

Samples from Germunde (North of Portugal, Ge-6 and Ge-7), described by Nieto (2002), and from black shales of the Iberian Range (ON-1), described by Bauluz and Nieto (2018), have been re-analysed by TEM using new more exact energy dispersive X-ray spectroscopy (EDX) methods to gain a better knowledge of their chemical composition at the nanoscale. They were prepared as ion-milled specimens for TEM analysis; copper rings were attached to areas of thin sections prepared with Canada balsam, selected in the rock matrix, apparently free of detrital grains. After being cut and detached from the thin section through gentle heating, they were ion-thinned using a Fischione-1050 ion mill and carbon-coated. Low-magnification and high-resolution images and SAED patterns were obtained at the Centro de Instrumentación Científica (CIC) of the Universidad de Granada (Spain) using two Thermo Fisher electron microscopes, with an XFEG emission gun, Titan, at 300 kV, with a spherical aberration corrector and TALOS at 200 kV, equipped with the Super-X system (four energy dispersion X-ray EDX detectors). X-ray elemental maps were acquired by scanning transmission electron microscopy (STEM) using a high-angle annular dark-field (HAADF) detector. The system allows the integration of all of the individual spectra of each map pixel to produce a spectra sum corresponding to selected polygons of the chemical maps. In this way, homogeneous areas may be chosen for quantitative analysis after the map has been registered. For quantitative micro-analyses, the EDX data were corrected in a first calculation using the thin-film method (Cliff and Lorimer, 1975). The anomalous results for K so obtained (see below in the Results section) suggested the calculation of a second set of data, corrected by absorption.

The absorption correction method is based on the electron neutrality criterion, which was developed by Van Cappelen and Doukhan (1994). The X-ray microanalysis software incorporates a routine to calculate an absorption correction factor. Using different fictitious thicknesses to process a particular spectrum, the calculated concentrations are plotted on a perfect parabola versus the chosen thickness. The thickness point at which the two parabolas representing the respective sums of positive and negative charges cross each other can be assumed to be the actual thickness for a final calculation. The latter implies that oxygen is analysed, and a $K_{O/Si}$ must also be determined (Conconi et al., 2023, 2025). The two sets of K factors (Cliff and Lorimer and 0-thickness) for the transformation of intensity ratios into concentration were determined using the following as standards: muscovite, biotite, albite, anorthite, anorthoclase, microcline, augite, olivine, scapolite, rhodonite, osumilite, spessartine, hemimorphite, and titanite.

Homogeneous chips of the rocks were used for the XRD analyses. The clay fraction ($< 2\,\mu m$) was extracted by centrifugation and extraction of supernatant liquid according to the Stokes's law. Oriented aggregates were prepared by sedimentation on glass slides. They were studied using a PANalytical X'Pert Pro diffractometer, with CuKα radiation, 45 kV and 40 mA, equipped with an X'Celerator solid-state linear detector. We used a step increment of 0.008° 2θ and an overall counting time of 10 s per step.

3 Computational methodology and models

The atomic coordinates of the crystal structure of tobelite were taken from the Mesto et al. (2012) structure, and the

$2 \times 1 \times 1$ supercells were modelled with 100 and 172 atoms, respectively. The theoretical calculations are based on the density functional theory (DFT). The optimisation process of these models was developed using the CASTEP code (Clark et al., 2005) included within the Materials Studio package (Materials Studio, 2025); plane waves and periodical boundary conditions were used. Electronic calculations were performed using the generalised gradient approximation (GGA) with PW91, PBE, and RPBE as exchange correlation functionals (Hammer et al., 1999; Perdew et al., 1996a, b). A mesh cut-off energy of 900 eV was used, along with on-the-fly-generated (OTFG) normal conserving pseudopotentials (Vanderbilt, 1990) with the relativistic treatment of Koelling–Harmon (Koelling and Harmon, 1977).

The convergence criterion for the self-consistent field was 1×10^{-6} eV per atom. On the other hand, for weak interactions, we applied the semiempirical (Tkatchenko and Scheffler, 2009) dispersion correction method by fully optimising with GGA/PBE/TS. This correction was applied to all crystal structures.

Models

To study the energetic stability of NH_4 micas as a function of the proportion of K^+ and NH_4^+ in the interlayer space, we employed two models, one of them in a unit cell to simulate the NH_4^+ proportion of the interlayer cation from 0 % (muscovite model), 25 %, 50 %, 75 %, and 100 % (tobelite model). However, to simulate an intermediate proportion of 12.5 %, we needed to increase the unit cell to $2 \times 1 \times 1$.

To determine the energetic stability in the tobelite composition in relation to K^+/NH_4^+ proportion, we used cation exchange energy:

$$E_{\text{exchange}} = \text{Sample}(\text{n}NH_4^+ \text{n}K^+) - (\text{tobelite}(4NH_4^+) - \text{n}NH_4^+ + \text{n}K^+), \quad (1)$$

where E_{exchange} is the cation exchange energy of the ammonium cation by the K^+ cation in the mineral structure, sample refers to the composition of the mixed sample (K^+/NH_4^+), tobelite is the energy of the sample with $4NH_4^+$, and nK^+ and nNH_4^+ are the number of cations exchanged in the mixed sample.

4 Results

4.1 Texture and chemical composition of coexisting micas

The Germunde and Iberian Range samples are formed by an intergrowth of phyllosilicates (Fig. 2), as fully described by TEM textural images, high-resolution TEM images, and electron diffraction patterns by Nieto (2002) and Bauluz and Nieto (2018). SAED patterns show examples of the $1M_d$ polytype (Fig. 2a – inset) and one- and two-layer polytypes (Fig. 2b – inset); the local order corresponding to a two-layer polytype also can be recognised in bi-dimensional high-resolution images (upper-left zone of Fig. 2a) of the area that globally produces a disordered polytype (Fig. 2a – inset).

The chemical maps obtained with EDX in STEM mode over the HAADF images of the mica-rich areas of samples Ge-6, Ge-7, and ON-1 show that they are formed by a nanometric intergrowth of K-rich and K-poor packets (Fig. 3), in coherence with the usual co-existence of the two micas in XRD diagrams (Nieto, 2002; Bauluz and Nieto, 2018; Bobos, 2019) (Fig. 1). The K-depleted areas are predominant, being in some areas the only kind of mica present. The K-rich areas are minor intercalated subparallel packets, with variable thickness, under the µm size. Together with the two kinds of micas, berthierine can also be recognised in some areas of samples Ge-6 and Ge-7 by its high Fe content (Fig. 3b).

The areas for quantitative analyses were selected on the previously obtained maps using ad hoc-drawn homogeneous polygonal zones to guarantee the absence of significant mutual contamination among the phases. Owing to its lower formation temperature, sample ON-1 has smaller-sized NH_4-rich and NH_4-free areas (Fig. 3; see scale); hence, the selection of adequate areas for analysis was particularly difficult, making the attainment of a larger number of areas free of mutual contamination challenging.

First, the analyses were processed using the thin-film approximation (Cliff and Lorimer, 1975). Formulae were adjusted to six tetrahedral + octahedral cations. Nevertheless, unrealistic K contents, significantly over the theoretical maximum of 1 atom per formula unit (apfu) for the interlayer position, were frequently obtained for the K-rich areas. Therefore, all analyses were re-processed using the absorption correction method proposed by Van Cappelen and Doukhan (1994) (see Sect. 2). Even so, some K-rich analyses (20 % of the whole population) failed to reach a coherent result (in these cases, the parabolas corresponding to negative and positive charges did not cross at all); those analyses were finally rejected. Figure 3 includes some representative formulae of the two kinds of micas for the three samples, and Table S1 in the Supplement shows the entire processed analyses.

Due to the limitation of quantitatively analysing NH_4 in EDX, its content must be indirectly evaluated by the interlayer deficit in the formula of the micas. Therefore, even if we have not attempted to quantify it by difference, due to multiple crystal–chemical uncertainties, the K-poor areas in Fig. 3 should represent the ammonium micas, and the overall interlayer sum in Table S1 gives the clue regarding separating the two kinds of micas. Figure 4 shows the ratios of this interlayer content (K + Na) in relation to the two major elements (Si and Al) in micas. Ratios between elements, better than absolute content, have been selected to avoid possible bias introduced by the adopted normalisation criterion.

The two types of micas recognised in the chemical maps (Fig. 3) define separated fields in Fig. 4, with the K-rich mi-

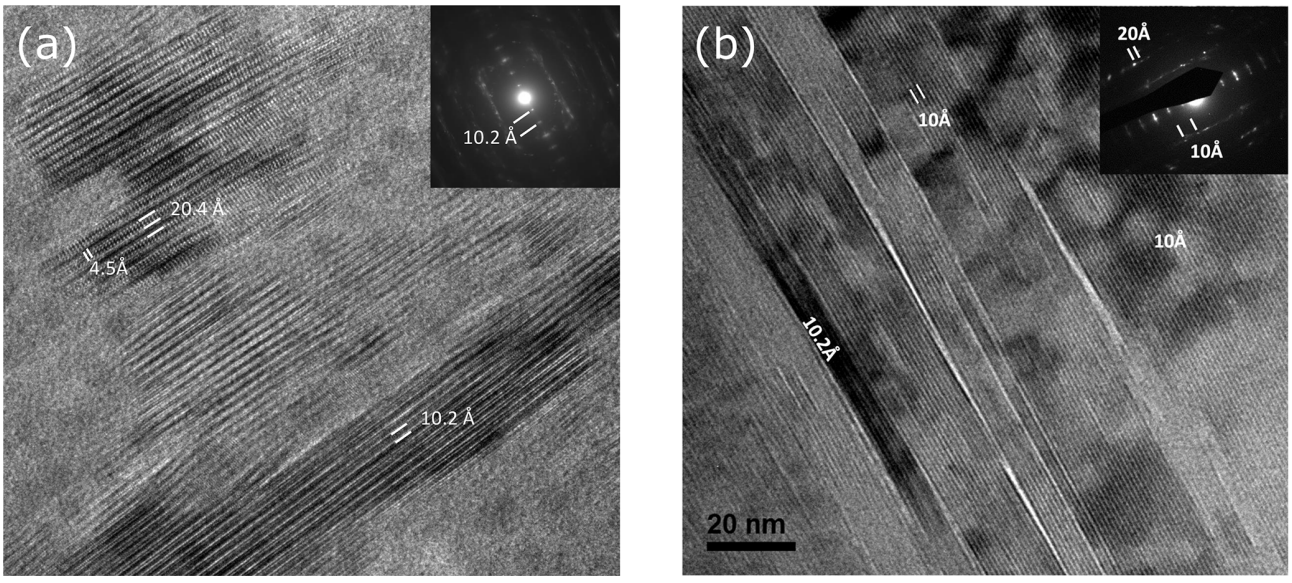


Figure 2. High-resolution transmission electron images and electron diffractions (insets) representative of the analysed samples. **(a)** NH_4 mica area of sample Ge-7. **(b)** Nanometric intergrowth between NH_4 (10.2 Å) and K (10 Å) micas of sample ON-1.

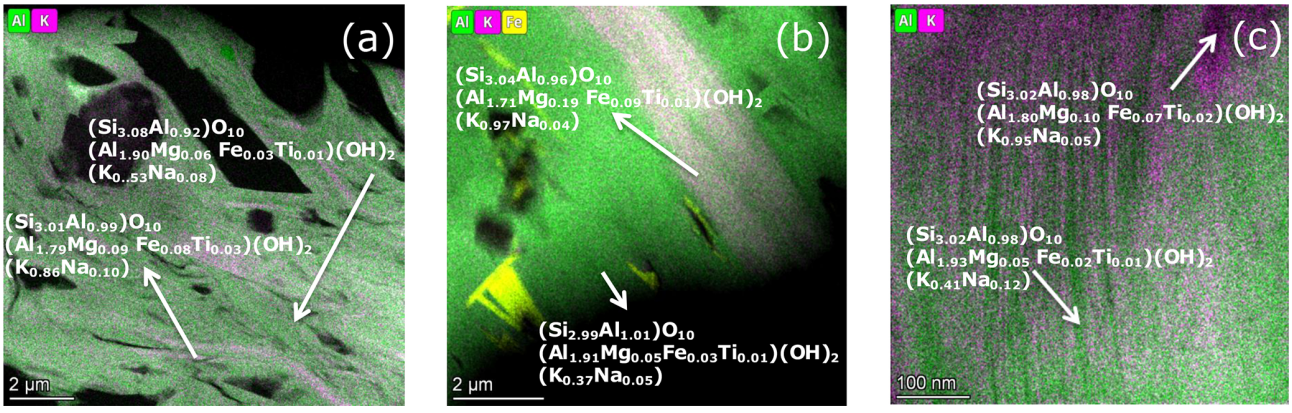


Figure 3. Chemical maps showing the nanometric intergrowth between NH_4 (green) and K (pink) micas. **(a)** Sample Ge-6. **(b)** Sample Ge-7 (yellow areas are berthierine). **(c)** Sample ON-1.

cas covering a relatively narrow field, coherent with the theoretical compositions of muscovite and illite (stars in Fig. 4). The NH_4 micas, represented by the K-poor areas, extend over a wider field, presumably indicating a wide range of NH_4 contents among samples, but also at the individual sample level.

When Mg is significantly present in the system, the corresponding phengitic content of the resulting micas is preferentially concentrated in the K micas over the corresponding NH_4 micas (Figs. 3 and 5).

4.2 The tobelite model – general structure

To reproduce the structure of tobelite and its energetic stability, three exchange correlation functionals, namely, PW91, RPBE, and PBE, were probed to select that which best reproduced the experimentally measured crystalline parameters in the literature. The unit cell of the monoclinic crystal of tobelite contains 100 atoms (Fig. 6). After full optimisation with each functional, the crystalline parameters a, b, and c and α, β, and γ angles were determined (Table 1).

The calculated crystalline parameters are close to the experimental ones, in particular, c and $csin\beta/2$, which are of the most sensitive parameters in this mineral, due to its dependence on the NH_4 content. The energetic stability of the tobelite unit cell model with each exchange correlation functional was analysed as a function of this parameter. Figure 7 shows that the energy is similar in all functionals, but $csin\beta/2$ calculated with the PBE functional is shorter than the rest of the functionals and is closer to the experimental $csin\beta/2$, determined by Mesto et al. (2012) (Table 1), the described one

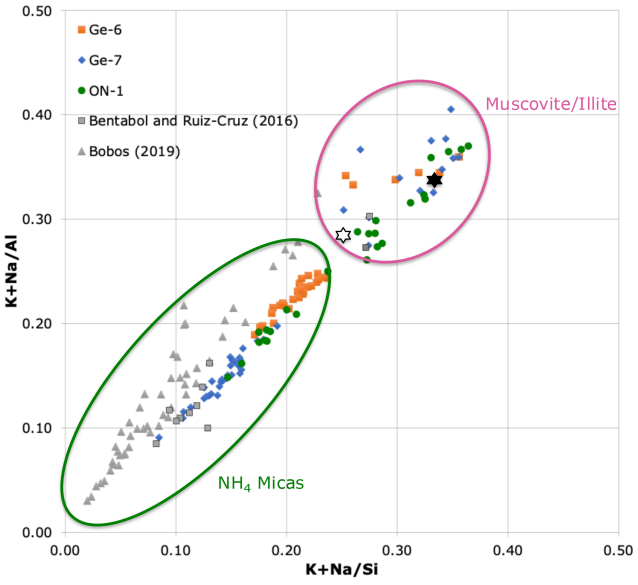


Figure 4. Chemical compositions of areas identified in HAADF maps as NH_4 micas and muscovite/illite (see Fig. 3). Note that both axes represent atomic ratios; hence, they are not affected by the normalisation criterion. Stars indicate the theoretical values for muscovite (black) and illite (white). The grey triangles represent the data of natural hydrothermal samples from Bobos (2019). The grey squares represent data from samples synthesised at 200 °C from Bentabol and Ruiz Cruz (2016b).

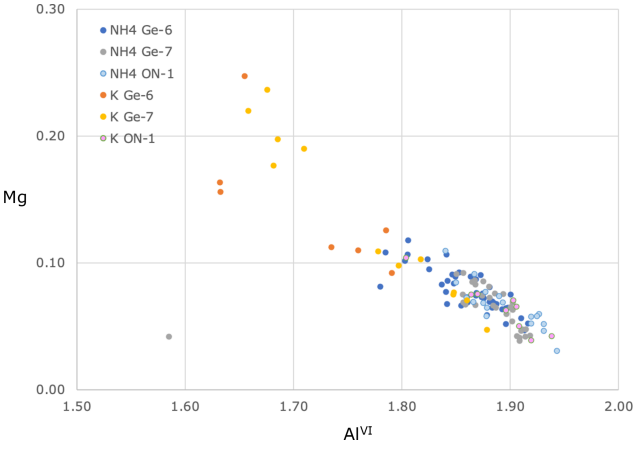


Figure 5. Comparison of the phengitic content (Al^{VI} vs. Mg) between ammonium (NH_4) and potassium (K) micas, separated according to their identification in Figs. 3 and 4.

by Higashi (2000) for pure tobelite (10.36 Å), and the calculated ones for the extreme-member tobelite using the equations by Drits et al. (1997) and Higashi (2000), which relate the NH_4 content with d_{001}, that is, $csin\beta/2$.

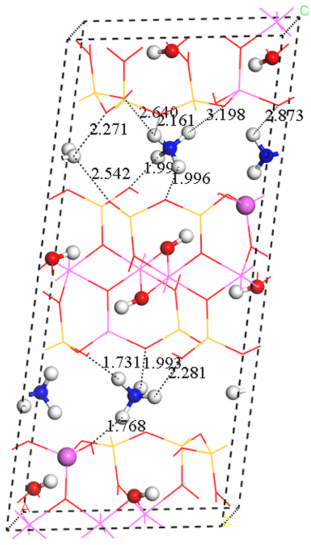


Figure 6. Tobelite crystal structure optimised under dry conditions. The H, O, Al^{IV}, and N atoms are represented by white, red, pink, and blue balls, respectively. Tetrahedral and octahedral Al, Si, and O atoms are represented as sticks in pink, yellow, and red colours, respectively. View from the (100) plane. These same representation criteria are used in the rest of the structural figures.

Table 1. Exchange correlation functional and optimised crystalline parameters in Å and degrees.

Functional	a	b	c	α	β	γ
PW91	9.07	5.24	21.05	88.85	99.22	90.07
RPBE	8.79	5.08	21.29	89.39	99.49	90.12
PBE	9.07	5.24	21.02	88.79	99.29	90.08
Experimental*	9.02	5.20	20.82		99.99	

* Mesto et al. (2012). $2M_2$ polytype. Note that the relative orientation of a and b parameters in the $2M_2$ polytype is changed in relation to the well-known one of the $2M_1$ polytype.

4.3 Energy evolution for different NH_4/K ratios

In these calculations, we simulated different NH_4/K ratios in the unit cell model: 75 % for $3NH_4$/K, 50 % for $2NH_4$/2K, 25 % for NH_4/3K (Fig. 8a, b and c), and 0 % for an ideal tobelite structure with four NH_4 as interlayer cations (Fig. 6). However, to simulate the smallest fraction of NH_4, we need to increase the unit cell size to $2 \times 1 \times 1$, which would allow 12.5 % NH_4 or 87.5 % K composition (NH_4/7K), as shown in Fig. 8d.

As with the aforementioned tobelite model, after full optimisation of all compositions, the $csin\beta/2$ parameter was determined for each composition in the unit cell and $2 \times 1 \times 1$ cell models (Fig. 9a). As expected, the theoretical calculation suggests that $csin\beta/2$ value decreases with K/NH_4 ratios, from ideal tobelite (K 0.0 %) to muscovite (K 100 %), with intermediate compositions of 25 %, 50 %, 75 %, and 87.5 % K-rich. On the other hand, the energetic stability increases

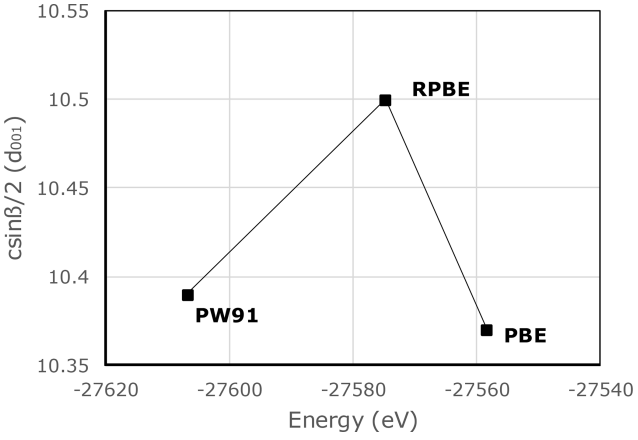


Figure 7. The energy behaviour of the tobelite crystal structure optimised with different exchange correlation functionals in relation to $csin\beta/2$ (d_{001}).

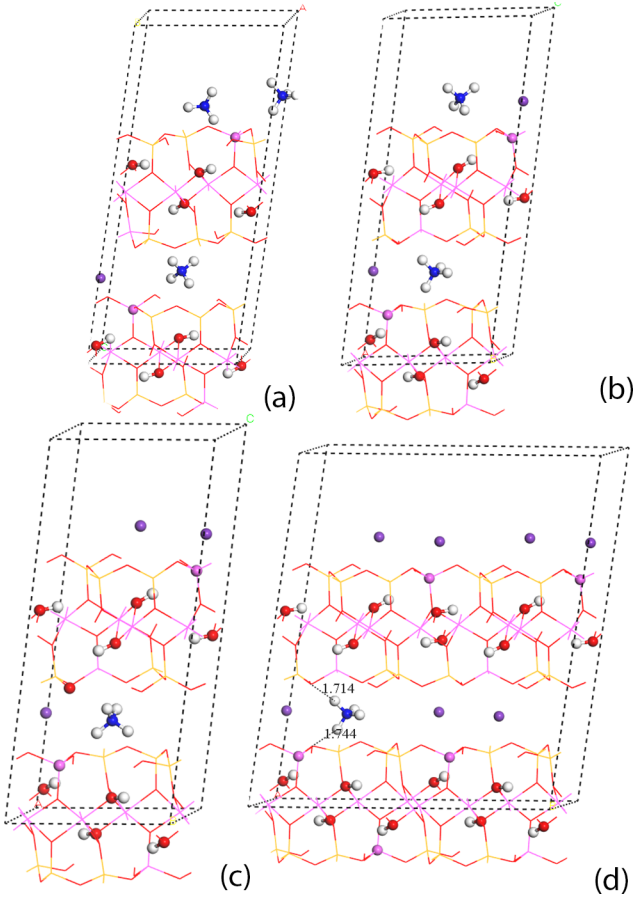


Figure 8. Optimised crystal structures of the NH_4/K tobelite compositions under dry conditions: **(a)** 75 % of NH_4, **(b)** 50 % of NH_4, and **(c)** 25 % of NH_4 (these are represented in unit cell) and **(d)** 12.5 % of NH_4, represented in $2 \times 1 \times 1$ cells. K atoms in purple.

in the compositional series from tobelite to muscovite (25 %, 50 %, 75 %, and 87.5 % K/(NH_4)), which is the opposite behaviour to that of the $csin\beta/2$.

In order to understand the energetic incorporation of the NH_4 molecule into the muscovite-to-tobelite series, we calculated the cation exchange energy for each composition. For instance, at 75 % K (NH_4/3K ratio), incorporating one ammonium ion into the structure requires −6.5 eV. When all of the K cations are removed to form the ideal tobelite mineral – the process requiring −25.66 eV – all of these processes are exothermic, and the resulting products are stable. However, anomalous behaviour is observed in the 87.5 % K composition (NH_4/7K): the cation exchange energy corresponds to one NH_4 group being incorporated but in the opposite sense (i.e. the value is +6.8 eV), indicating an endothermic process. (Fig. 9b).

4.4 Hydrogen bonds and electrostatic repulsions

The hydrogen bonds between the protons of the ammonium ion and the tetrahedral oxygen atoms, as well as the electrostatic repulsion between the nitrogen of the ammonium group and the tetrahedral oxygen atoms, may be important for understanding the driving forces behind the composition ratio in this group of minerals.

The interaction distances of the hydrogen bonds (H…O) and N…O repulsion distances were determined for each optimised structure of the NH_4/K ratios described above, using the radial distribution function (RDF) available in Materials Studio's analysis software. The obtained RDF plots reveal consistent behaviour in all compositions; i.e. the hydrogen bond distance (H…O) remains close to 1.7–2.5 Å. These values are consistent with previous theoretical calculations relating to hydrogen bonds in clay minerals, as well as adsorption processes in olivine (Escamilla-Roa et al., 2014; Escamilla-Roa and Sainz-Díaz, 2014). The repulsion distance between N and the tetrahedral O atoms varies from 2.8 to 3.5 Å.

The RDF graph analysis does not show a clear effect on the geometric features of hydrogen bonds and electrostatic repulsion in environments with different NH_4/K ratios. We used the statistical RStudio software (Posit team, 2025) to determine the main interaction distance values from the RDF database that correspond to the highest-frequency peaks. These values are summarised in Table 2, which shows the composition in each sample (NH_4/K proportion), the cation exchange energy, the RDF (H..O and N..O) major peaks, and the $csin\beta/2$ parameter.

The shorter hydrogen bond interaction value (H…O = 1.7 Å) corresponds to the composition (NH_4/7K), which is consistent with the $csin\beta/2$ shorter than those of the tobelite compositions. The NH_4^+ cation is in a compact environment with close oxygen atoms. Therefore, the main peak corresponds to the strongest hydrogen bonds. However, in samples with a high proportion of NH_4^+, the value

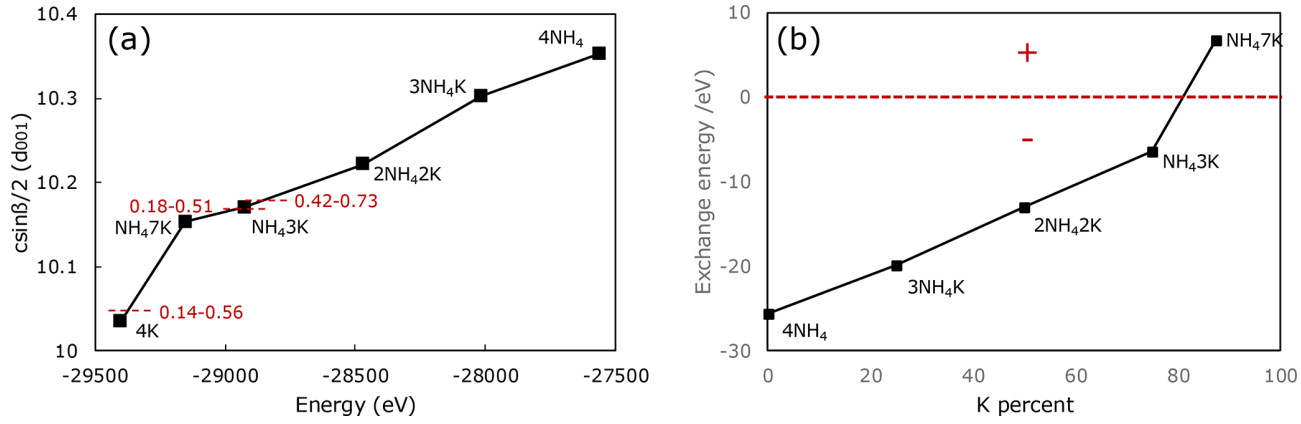


Figure 9. **(a)** Energy and $csin\beta/2$ behaviour of the optimised tobelite/muscovite compositional series structures. Dashed horizontal red lines indicate the experimentally measured d_{001} of the studied samples (data from Nieto, 2002; Bauluz and Nieto, 2018), and red numbers indicate the range of NH_4 content determined in this study (see Table S1). **(b)** NH_4 cation exchange energy at different K cation percentages in the tobelite compositional series, showing the change from negative to positive exchange energy for the NH_4/7K composition.

oscillates between 3.33 Å for the tobelite sample and 2.8 Å for the $1NH_4/3K$ sample (75 % K ratio).

The analysis of the main repulsion distances between the nitrogen atoms of NH_4^+ and the interlayer tetrahedral oxygen atoms suggests that, from tobelite ($4NH_4$) to samples with lower NH_4^+ content ($1NH_4/3K$), the distance decreases from 3.47 to 2.85 Å. Samples with a low proportion of NH_4^+ exhibit weaker repulsive interactions. Conversely, the sample with 87.5 % K content exhibited the main peak at 3.39 Å; this value is similar to that of the tobelite sample, suggesting a more repulsive environment. This composition exhibits the opposite behaviour compared to the aforementioned series (0 %–75 % K ratio).

5 Discussion

5.1 The structure of NH_4-rich micas – new details from the computer calculations

The calculated structure for tobelite- and NH_4-bearing micas (Figs. 6 and 8) reproduces the well-known organisation of the TOT layer of dioctahedral micas and, in general, the dioctahedral phyllosilicates. This result was also obtained in previous first-principles studies of ammonium micas (Geatches et al., 2014; Yu et al., 2016), which also emphasised the significance of the H bonds. Yu et al. (2016) also considered the influence of the type of tetrahedral cations (Si and/or Al) surrounding the NH_4 cation. The obtained result also coincides with the existing structural determinations on single-crystal specimens of tobelite and NH_4 micas by Mesto et al. (2012) and on powder samples, using Rietveld methods, by Harlov et al. (2001) and Poter et al. (2007). Finally, according to the cited experimental determinations and the theoretical results, the interlayer space is the only significant difference compared to muscovite, phengite, or illite due to the total or partial substitution of K by NH_4. The change of a single cation by a molecule increases this space in proportion to the NH_4/K ratio and opens the possibility of connections between the H of the molecule and the basal O of the tetrahedral sheet.

In fact, Mesto et al. (2012) showed that the differences in the basal spacing ($csin\beta$) of micas with interlayer cations of different sizes are exclusively dependent on the interlayer thickness (Fig. 7 in Mesto et al., 2012); that is, the TOT layer has a nearly fixed width, with the overall thickness of the structure changing only in response to the size of the interlayer cation (Fig. 10a). This general rule also applies for the NH_4-bearing micas and includes different polytypes ($2M_1$ vs. $2M_2$). This close dependence between interlayer thickness and cation size constitutes the basis for the formulae proposed by Drits et al. (1997) and Higashi (2000), which relate NH_4/K ratios with the basal spacing. Figure 9a shows the evolution of the basal spacing with NH_4 content for the calculated structures.

The tetrahedral rotation angle is another structural characteristic closely linked to the size of the interlayer cation. This is the angle by which the ditrigonal rings of the TOT layer's basal oxygen plane deviate from the ideal hexagonal geometry. In general, this angle is higher (more distorted) for small cations, such as Na, but approximates the ideal hexagonal character for large cations, such as Cs (Fig. 10b), because these cations require more space in the ring. Therefore, the relationship between the tetrahedral rotation angle and the interlayer thickness for Na, K, and Cs micas follows a nearly linear tendency. Nevertheless, NH_4-bearing mica and tobelite deviate from this general trend, having a tetrahedral rotation angle very similar to that of muscovite despite their greater average interlayer cation size and thickness (Fig. 10b). In other words, NH_4 does not occupy the ditrigonal space in a manner similar to that of the spherical cations because of its

Table 2. Behaviour of hydrogen bonds between NH_4...O-tetrahedral layers and distances (N...O) of the optimised crystalline structures from NH_4 micas with different NH_4/K ratios. The RDF bond distance is in Å, and the cation exchange energy of each NH_4 molecule is in eV.

Composition	% K	Cation exchange energy	RDF major peak N...O	RDF major peak H...O	$csin\beta/2$
$4NH_4$	0.0	−25.66	3.47	3.33	10.35
$3NH_4$/K	25	−19.90	2.75	3.97	10.30
$2NH_4$/2K	50	−13.00	2.93	3.12	10.22
$1NH_4$/3K	75	−6.49	2.85	2.8	10.17
NH_4/7K	87.5	6.81	3.39	1.7	10.15

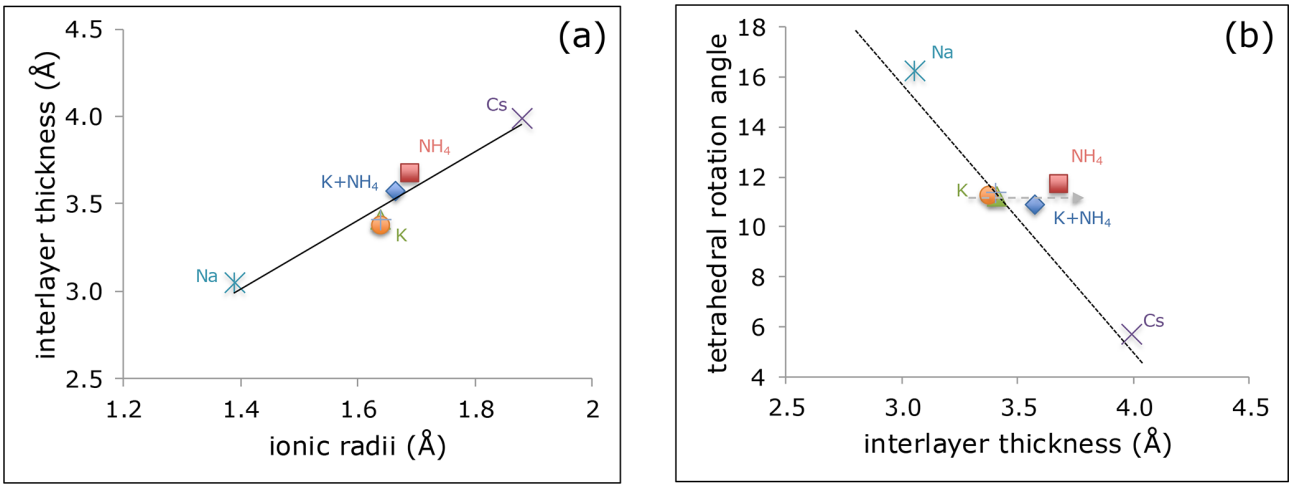


Figure 10. **(a)** Interlayer thickness in different micas depends on the ionic radius of the main interlayer cation. **(b)** Relationship between interlayer thickness and tetrahedral rotation angle. Note that NH_4-bearing micas deviate from the general tendency (dotted black line), maintaining the same angle as muscovite (dashed grey arrow). Data (interlayer thickness and tetrahedral rotation angle) from Brigatti (1998) for $2M_1$ muscovites, from Zhoukhlistov et al. (1973) for $2M_2$ phengite, from Ni and Hughes (1996) for $2M_2$ nanpingite, from Lin and Bailey (1984) for $2M_1$ paragonite, and from Mesto et al. (2012) for tobelite and NH_4-muscovite. Ionic radii from Shannon (1976) and Pöter (2003).

tetrahedral geometry and the capacity to establish hydrogen bonds with the basal oxygens of the ring (Fig. 6).

In conclusion, the structural organisation of tobelite and NH_4 micas is similar to that of other micas (e.g. muscovite), but the presence of H in the ammonium molecule allows the existence of H bridges. These weak bonds complement the general electrostatic attraction between the positively charged ammonium and the TOT layer, which is the main stabilising link of the mica structure. The exact location of the H atoms in the structure has been precluded until now by their extremely light electronic density and the low-crystallinity character of all of the samples experimentally determined by both single-crystal and powder methods. Therefore, the theoretical approximation carried out in this study produces the only possible data on the predictable location of the H atoms and the existence of H bonds, which, in addition, probably help to stabilise the structure up to its collapse for the K_7/NH_4 composition, which becomes energetically unfavourable (Fig. 9b and Table 2).

One consequence of the H bonds is the possibility of stabilising polytypes different from $2M_1$, which is typical in mature rock-forming dioctahedral micas. Other polytypes have been described for dioctahedral micas, but they are rare, restricted to particular compositions, as in the case of 1M (Peacor et al., 2002), or disordered, as in the case of the $1M_d$ in illites progressively evolving to mature micas (Chen and Wang, 2007; Nieto et al., 2010). In other phyllosilicates, such as the kaolinite group or chlorites, the H bridges play a crucial role in the variety and nature of the polytypes. According to the cited structural XRD determinations and SAED data in the literature, various polytypes (1M, $1M_d$, $2M_1$, $2M_2$, 3T, and 2Or) coexist in NH_4-rich micas at the sample level, and $2M_2$ was the predominant polytype determined on the single crystals analysed by Mesto et al. (2012), with local coexistence with other polytypes (Capitani et al., 2016). Therefore, the existence of H bridges could open the possibility of different polytypes. Small energetic differences among them for NH_4-rich micas, together with the low activation energy at the low temperatures at which they form, could be responsible for their usual coexistence in all of the studied samples, linked or not, to the particular composition of each grain.

5.2 Coexistence of extreme muscovite (or illite) and NH_4-bearing micas

In many natural occurrences of tobelite or NH_4-bearing micas, these coexist with illite or muscovite at the sample level (Juster et al., 1987; Nieto, 2002; Bauluz and Nieto, 2018; Bobos, 2019). This coexistence was also the result of the NH_4–micas synthesised by Bentabol and Ruiz Cruz (2016b). Due to their slightly different basal spacing and intensity ratios, the two micas produce differentiated XRD peaks (Fig. 1), similarly to the coexistence between muscovite and paragonite, the Na-bearing mica. In such cases, the basal spacing of the NH_4-bearing mica is dependent on its content of NH_4 (Drits et al., 1997; Higashi, 2000), but the position of the K mica peak is fixed, corresponding to its characteristic 10 Å spacing. This study confirms the coexistence of the two micas at the nanoscale level (Figs. 2 and 3) using HAADF images and chemical EDX maps in coherence with previous TEM images described by Nieto (2002), Bauluz and Nieto (2018), and Bobos (2019). Quantitative analysis revealed that the two phases define different compositional fields, one interlayer deficient due to the lack of NH_4 data and the other with nearly full occupancy of the interlayer space, giving typical formulae of K micas in the field of illite or muscovite (Table S1 and Fig. 4). Even if the K micas scatter between the theoretical compositions of illite and muscovite, they define a limited range of compositions, which is consistent with the one described in the literature and acknowledged in the IMA classification of micas (Rieder et al., 1998).

On the other hand, the coexisting NH_4-bearing micas extend over a wide range of compositions, variable from sample to sample but also dependent on the analysis point for any given sample (Fig. 4). This range extends from nearly extreme tobelite up to NH_4-bearing muscovite, defining the existence of a continuous solid solution between the two extremes in structural and thermodynamic terms. Nevertheless, the K-rich endmember of this continuous solid solution is not pure muscovite but a term richer in K, although it still contains significant NH_4. This continuous solid solution is consistent with the structural determinations of single crystals of tobelite and NH_4-rich muscovite by Mesto et al. (2012), in which no significant structural differences were found between the two crystals, with only the expected differences in structural parameters due to the nature of the major interlayer cation, NH_4 vs. K.

Based on the structural description and energy stability calculations performed in this study, NH_4 can enter the mica structure as an interlayer cation, coexisting with variable proportions of K from the endmember tobelite up to, at least, a proportion of 75 %K / 25 % NH_4. In this range, both the variation of energy and the basal spacing show a continuous behaviour (Fig. 9), with the two properties varying linearly depending on the K/NH_4 ratio. This continuous behaviour allows the determination of the NH_4 content based on the experimentally measured basal spacing (Drits et al., 1997; Higashi, 2000). In all of this solid solution, the incorporation of K into the tobelite structure is energetically favourable (Fig. 9), possibly due to the effect of shorter H bonds (Table 2). Nonetheless, the calculated structure for 87.5 %K / 12.5 % NH_4 shows a change to positive energy (Fig. 9b), making such composition unfavourable in relation to a pure mixture of NH_4-rich muscovite (or tobelite) and NH_4-free muscovite. Interestingly, this composition coincides with the absence of analytical data between the NH_4-bearing micas and the illites/muscovites (Fig. 4).

The energetic and structural calculations presented in this study, producing the above described continuity, are based on the structure of the $2M_2$ polytype of micas as this was the major polytype determined by Mesto et al. (2012) for both tobelite and NH_4-rich muscovite single crystals and one of those present in the mixture of polytypes in powder samples, determined by means of the Rietveld method by Harlov et al. (2001) and Poter et al. (2007). This mixture of polytypes seems to be a characteristic of NH_4-bearing micas as it has also been described in TEM studies (Nieto, 2002; Bentabol and Ruiz Cruz, 2016b; Bauluz and Nieto, 2018; Bobos, 2019) and contrasts with the ubiquitous presence of the $2M_1$ polytype of muscovites and phengites in nature. Therefore, the structural differences between NH_4-bearing and NH_4-free micas cause differences in the stability of the polytypes, for which the importance of H bridges in NH_4-bearing micas may produce the stabilisation of polytypes different from $2M_1$.

Given that the solid solution between NH_4 and K micas extends over a wide range of compositions, those sample zones in which the proportion between the two main interlayer cations is inside the solid-solution field produce micas with mixed compositions. As it is characteristic of low-temperature rocks (Morse and Casey, 1988; Merriman and Peacor, 1999), these diagenetic and very-low-grade metamorphic samples have not reached chemical equilibrium, which justifies the large range of compositions at the level of individual samples. Such internal differences are even present inside single crystals (Capitani et al., 2016). Only those areas in which the proportion between the two cations corresponds to a higher K content than that acceptable in the structure of NH_4-bearing micas solve this forbidden composition by exsolving a minor quantity of muscovite or illite. These areas deal with the energetic problem of micas having a composition near the K endmember but with a minor proportion of NH_4 by the coexistence of two different micas, which is energetically more favourable.

6 Conclusions and implications for mica nomenclature

Ammonium-bearing micas share the general structure with other micas, particularly regarding the TOT layer organisation, but have their particularities concerning the interlayer

space. The tetrahedral geometry of the NH_4 ion results in a different behaviour compared to usual spherical ions, opening the possibility of interactions between the H atoms of the molecule and the basal oxygens of the TOT layer. Such a different geometry and type of bonding affects the tetrahedral rotation angle, for which NH_4 micas deviate from the general tendency that relates the interlayer cation size and the tetrahedral rotation angle, with ammonium micas having a bigger distortion than what it would correspond to according to their cation size. These interlayer space configuration differences affect the relative stability of polytypes. Unlike muscovite, NH_4 micas in nature combine various polytypes at the sample level without a defined typical polytype.

Density functional calculations have shown that ammonium micas are continuously stable over a wide range of NH_4/K ratios from the NH_4 endmember, tobelite, up to compositions with K as the major interlayer cation; however, the composition near 87.5 % K becomes energetically unfavourable, showing positive cation exchange energy. Compositional maps and quantitative analyses obtained using analytical electron microscopy over HAADF images have shown that those compositions near the K endmember but still with a significant proportion of NH_4 are absent in nature. Areas with this type of composition are formed by a nanometric intergrowth of NH_4 micas and muscovite or illite.

In conclusion, NH_4 micas are a solid solution covering a wide field of NH_4/K ratios and should be considered to be a series name, with tobelite as their NH_4 endmember. The K-rich endmember of the solid solution still contains a significant NH_4 content; hence, it is not muscovite; its exact composition is difficult to know exactly due to analytical uncertainties and the possible influence of physical–chemical genetic conditions. Moreover, NH_4 mica series and muscovite have minor structural differences, which justifies the existence of a compositional gap between them. These differences are related to the organisation of the interlayer space due to the tetrahedral geometry of the NH_4 molecule and the existence of H bonds with the TOT layer's basal oxygen atoms.

Data availability. All relevant data are displayed in the article, and the Supplement and additional data are available upon request from the corresponding author.

Supplement. The supplement related to this article is available online at https://doi.org/10.5194/ejm-38-655-2026-supplement.

Author contributions. FN designed the original idea for the study. EER and VT conducted all of the calculations and the interpretation of the theoretical results. FN and BB performed the electron microscopic observations. JP and MMA processed and prepared the analytical electron microscopy data. FN and EER prepared the original paper. All of the authors discussed the analytical results and reviewed the paper.

Competing interests. The contact author has declared that none of the authors has any competing interests.

Disclaimer. Publisher's note: Copernicus Publications remains neutral with regard to jurisdictional claims made in the text, published maps, institutional affiliations, or any other geographical representation in this paper. The authors bear the ultimate responsibility for providing appropriate place names. Views expressed in the text are those of the authors and do not necessarily reflect the views of the publisher.

Acknowledgements. We acknowledge the technical and human support provided by the Centro de Instrumentación Científica of the Universidad de Granada; in particular, Cecilia de la Prada is recognised for helping with the work in the Talos microscope, and Daniel García Muñoz Bautista Cerro and Javier Jáimez Águila are acknowledged for the ion-milling preparation of samples. Josefina Pedrajas acknowledges the Research Project B-CIC-006-UGR23, co-financed by the Department of University, Research and Innovation and the European Union under the FEDER Andalusia programme 2021–2027. The authors acknowledge the CTI (CSIC) and CESGA for providing the computing facilities. The publication fees were covered by an aid of the Sociedad Española de Mineralogía. The editors and Javier Huertas and another anonymous reviewer are acknowledged for the careful revision and handling of the paper.

Financial support. This research has been supported by the Ministerio de Ciencia, Innovación y Universidades (grant nos. PID2021-1231270B-I00, PID2023-147440OB-C22, PID2024-158529NB-I00, and B-CIC-006-UGR23) and the Junta de Andalucía, Consejería de Universidad, Investigación e Innovación, Junta de Andalucía (grant nos. FEDER-UJA Andalucía 2021-2027.M.1.B.B TA_000655 and Research Group RNM-179).

Review statement. This paper was edited by Martine Buatier and reviewed by F. Javier Huertas and one anonymous referee.

References

Ammannito, E., Desanctis, M. C., Ciarniello, M., Frigeri, A., Carrozzo, F. G., Combe, J. P., Ehlmann, B. L., Marchi, S., McSween, H. Y., Raponi, A., Toplis, M. J., Tosi, F., Castillo-Rogez, J. C., Capaccioni, F., Capria, M. T., Fonte, S., Giardino, M., Jaumann, R., Longobardo, A., Joy, S. P., Magni, G., McCord, T. B., McFadden, L. A., Palomba, E., Pieters, C. M., Polanskey, C. A., Rayman, M. D., Raymond, C. A., Schenk, P. M., Zambon, F., and Russell, C. T.: Distribution of phyllosilicates on the surface of Ceres, Science, 353, https://doi.org/10.1126/science.aaf4279, 2016.

Bauluz, B. and Nieto, F.: Ammonium-bearing micas in very low-grade metapelites: micro- and nano-texture and composition, Clay Miner., 53, 105–116, https://doi.org/10.1180/clm.2018.8, 2018.

Bentabol, M. and Ruiz Cruz, M. D.: Characterization of tobelite formed from kaolinite under hydrothermal conditions (200 °C), Appl. Clay Sci., 126, 160–172, https://doi.org/10.1016/j.clay.2016.01.053, 2016a.

Bentabol, M. and Ruiz Cruz, M. D.: NH_4 for K substitution in dioctahedral mica synthesized at 200 °C, Appl. Clay Sci., 126, 268–277, https://doi.org/10.1016/j.clay.2016.03.025, 2016b.

Bobos, I.: Characterization of smectite to NH_4-illite conversion series in the fossil hydrothermal system of Harghita Bãi, East Carpathians, Romania, Am. Mineral., 97, https://doi.org/10.2138/am.2012.3801, 2012.

Bobos, I.: Coexisting nanoscale phases of K-illite, NH_4, K-illite and NH_4-illite-smectite: an organic nitrogen contribution in the hydrothermal system of Harghita Bãi, East Carpathians, Romania, Clay Miner., 54, https://doi.org/10.1180/clm.2019.4, 2019.

Brigatti, M. F.: Crystal chemistry of Mg-, Fe-bearing muscovites-2M, Am. Mineral., 83, https://doi.org/10.2138/am-1998-7-809, 1998.

Capitani, G. C., Schingaro, E., Lacalamita, M., Mesto, E., and Scordari, F.: Structural anomalies in tobelite-2M 2 explained by high resolution and analytical electron microscopy, Mineral. Mag., 80, 143–156, https://doi.org/10.1180/minmag.2015.079.7.14, 2016.

Chen, T. and Wang, H. J.: Determination of layer stacking microstructures and intralayer transition of illite polytypes by high-resolution transmission electron microscopy (HRTEM), Am. Mineral., 92, 926–932, https://doi.org/10.2138/am.2007.2293, 2007.

Clark, S. J., Segall, M. D., Pickard, C. J., Hasnip, P. J., Probert, M. I. J., Refson, K., and Payne, M. C.: First principles methods using CASTEP, Zeitschrift für Krist.-Cryst. Mater., 220, 567–570, https://doi.org/10.1524/zkri.220.5.567.65075, 2005.

Cliff, G. and Lorimer, G. W.: The quantitative analysis of thin specimens, J. Microsc., 103, https://doi.org/10.1111/j.1365-2818.1975.tb03895.x, 1975.

Conconi, R., Ventruti, G., Nieto, F., and Capitani, G.: TEM-EDS microanalysis: Comparison among the standardless, Cliff & Lorimer and absorption correction quantification methods, Ultramicroscopy, 254, 113845, https://doi.org/10.1016/j.ultramic.2023.113845, 2023.

Conconi, R., Abad Ortega, M. M., Nieto, F., Buono, P., and Capitani, G.: TEM-EDS microanalysis: Comparison between different electron sources, accelerating voltages and detection systems, Ultramicroscopy, 276, 114201, https://doi.org/10.1016/j.ultramic.2025.114201, 2025.

Drits, V. A., Lindgreen, H., and Salyn, A. L.: Determination of the content and distribution of fixed ammonium in illite-smectite by X-ray diffraction: Application to North Sea illite-smectite, Am. Mineral., 82, https://doi.org/10.2138/am-1997-1-210, 1997.

Escamilla-Roa, E. and Sainz-Díaz, C. I.: Effect of Amorphous Ammonia-Water Ice onto Adsorption of Glycine on Cometary Dust Grain and IR Spectroscopy, J. Phys. Chem. C, 118, 26080–26090, https://doi.org/10.1021/jp507650w, 2014.

Escamilla-Roa, E., Hernández-Laguna, A., and Sainz-Díaz, C. I.: Theoretical study of the hydrogen bonding and infrared spectroscopy in the cis-vacant polymorph of dioctahedral 2:1 phyllosilicates, J. Mol. Model., 20, 2404, https://doi.org/10.1007/s00894-014-2404-4, 2014.

Geatches, D., McCarty, D., and Wilcox, J.: Ab initio investigations of dioctahedral interlayer-deficient mica:Modeling particles of illite found within gas shale, Am. Mineral., 99, 1962–1972, https://doi.org/10.2138/am-2014-4868, 2014.

Guidotti, C. V., Sassi, F. P., Blencoe, J. G., and Selverstone, J.: The paragonite-muscovite solvus: I. P-T-X limits derived from the Na-K compositions of natural, quasibinary paragonite-muscovite pairs, Geochim. Cosmochim. Ac., 58, 2269–2275, https://doi.org/10.1016/0016-7037(94)90009-4, 1994.

Hammer, B., Hansen, L. B., and Nørskov, J. K.: Improved adsorption energetics within density-functional theory using revised Perdew-Burke-Ernzerhof functionals, Phys. Rev. B, 59, 7413–7421, https://doi.org/10.1103/PhysRevB.59.7413, 1999.

Harlov, D. E., Andrut, M., and Poter, B.: Characterisation of tobelite $(NH_4)Al\text{-}2\ AlSi_3O_{10}\ (OH)(2)$ and ND4-tobelite $(ND_4)Al\text{-}2\ AlSi_3O_{10}\ (OD)(2)$ using IR spectroscopy and Rietveld refinement of XRD spectra, Phys. Chem. Miner., 28, 268–276, 2001.

Higashi, S.: Tobelite, a new ammonium dioctahedral mica., Mineral. J., 11, https://doi.org/10.2465/minerj.11.138, 1982.

Higashi, S.: Ammonium-bearing mica and mica/smectite of several pottery stone and pyrophyllite deposits in Japan: Their mineralogical properties and utilization, Appl. Clay Sci., 16, 171–184, https://doi.org/10.1016/S0169-1317(99)00052-6, 2000.

Juster, T. C., Brown, P. E., and Bailey, S. W.: NH4-bearing illite in very low grade metamorphic rocks associated with coal, northeastern Pennsylvania, Am. Mineral., 72, 555–565, 1987.

Koelling, D. D. and Harmon, B. N.: A technique for relativistic spin-polarised calculations, J. Phys. C, 10, 3107, https://doi.org/10.1088/0022-3719/10/16/019, 1977.

Lin, C. Y. and Bailey, S. W.: The crystal structure of paragonite-2M1, Am. Mineral., 69, 1984.

Materials Studio: Materials Studio BIOVIA, Dassault Systèmes, Dassault Systèmes, San Diego, https://www.3ds.com/products/biovia (last access: 15 June 2026), 2025.

Merriman, R. J. and Peacor, D. R.: Very Low Grade Metapelites: mineralogy, microfabrics and measuring reaction progress, in: Low-Grade Metamorphism, edited by: Frey, M. and Robinson, D., Blackwells Science, Oxford, 10–60, ISBN 0-632-04756-9, https://doi.org/10.1002/9781444313345.ch2, 1999.

Mesto, E., Scordari, F., Lacalamita, M., and Schingaro, E.: Tobelite and NH_4^+-rich muscovite single crystals from Ordovician Armorican sandstones (Brittany, France): Structure and crystal chemistry, Am. Mineral., 97, 1460–1468, https://doi.org/10.2138/am.2012.4023, 2012.

Morse, J. W. and Casey, W. H.: Ostwald processes and mineral paragenesis in sediments, Am. J. Sci., 288, 537–560, https://doi.org/10.2475/ajs.288.6.537, 1988.

Ni, Y. and Hughes, J. M.: The crystal structure of nanpingite-2M2, the Cs end-member of moscovite, Am. Mineral., 81, https://doi.org/10.2138/am-1996-1-213, 1996.

Nickel, E. H.: Solid solutions in mineral nomenclature, Mineral. Petrol., 46, 49–53, https://doi.org/10.1007/BF01160701, 1992.

Nieto, F.: Characterization of coexisting NH_4^- and K-micas in very low-grade metapelites, Am. Mineral., 87, 205–216, https://doi.org/10.2138/am-2002-2-302, 2002.

Nieto, F., Mellini, M., and Abad, I.: The Role of H3O+ in the Crystal Structure of Illite, Clays Clay Miner., 58, 238–246, https://doi.org/10.1346/CCMN.2010.0580208, 2010.

Peacor, D. R., Bauluz, B., Dong, H., Tillick, D., and Yan, Y.: Transmission and analytical electron microscopy evidence for high Mg contents of 1M illite: Absence of 1M polytypism in normal prograde diagenetic sequences of pelitic rocks, Clays Clay Miner., 50, 757–765, https://doi.org/10.1346/000986002762090281, 2002.

Perdew, J. P., Burke, K., and Wang, Y.: Generalized gradient approximation for the exchange-correlation hole of a many-electron system, Phys. Rev. B, 54, 16533–16539, https://doi.org/10.1103/PhysRevB.54.16533, 1996a.

Perdew, J. P., Burke, K., and Ernzerhof, M.: Generalized Gradient Approximation Made Simple, Phys. Rev. Lett., 77, 3865–3868, https://doi.org/10.1103/PhysRevLett.77.3865, 1996b.

Posit team: RStudio: Integrated Development Environment for R, http://www.posit.co (last access: 30 March 2026), 2025.

Pöter, B.: Experimentally determined K-NH4 partitioning between feldspars, muscovites and aqueous chloride solutions, University of Berlin, Berlin, Germany, 102 pp., https://gfzpublic.gfz.de/pubman/item/item_229403 (last access: 23 October 2026), 2003.

Poter, B., Gottschalk, M., and Heinrich, W.: Crystal-chemistry of synthetic K-feldspar-buddingtonite and muscovite-tobelite solid solutions, Am. Mineral., 92, 151–165, 2007.

Rieder, M., Cavazzini, G., D'yakonov, Y. S., Frank-Kamenetskii, V. A., Gottardi, G., Guggenheim, S., Koval', P. W., Müller, G., Neiva, A. M. R., Radoslovich, E. W., Robert, J.-L., Sassi, F. P., Takeda, H., Weiss, Z., and Wones, D. R.: Nomenclature of the Micas, Clays Clay Miner., 46, 586–595, https://doi.org/10.1346/CCMN.1998.0460513, 1998.

Shannon, R. D.: Revised effective ionic radii and systematic studies of interatomic distances in halides and chalcogenides, Acta Crystallogr. Sect. A, 32, https://doi.org/10.1107/S0567739476001551, 1976.

Tkatchenko, A. and Scheffler, M.: Accurate molecular van der Waals interactions from ground-state electron density and free-atom reference data, Phys. Rev. Lett., 102, 073005, https://doi.org/10.1103/PhysRevLett.102.073005, 2009.

Van Cappelen, E. and Doukhan, J. C.: Quantitative transmission X-ray microanalysis of ionic compounds, Ultramicroscopy, 53, 343–349, 1994.

Vanderbilt, D.: Soft self-consistent pseudopotentials in a generalized eigenvalue formalism, Phys. Rev. B, 41, 7892–7895, https://doi.org/10.1103/PhysRevB.41.7892, 1990.

Yu, C. J., Choe, S. H., Jang, Y. M., Jang, G. H., and Pae, Y. H.: First-principles study of organically modified muscovite mica with ammonium (NH4+) or methylammonium (CH3NH3+) ion, J. Mater. Sci., 51, 10806–10818, https://doi.org/10.1007/s10853-016-0292-y, 2016.

Zhoukhlistov, A. P., Zvyagin, B. B., Soboleva, S. V., and Fedotov, A. F.: The crystal structure of the dioctahedral mica 2M2 determined by high voltage electron diffraction, Clays Clay Miner., 21, https://doi.org/10.1346/CCMN.1973.0210606, 1973.